Time-Scale Hybrid Continuous-Discrete Sliding Frank-Wolfe Method

Clara Lage, Nelly Pustelnik, Jean-Michel Arbona, Benjamin Audit

Space-Scale Hybrid Continuous-Discrete Sliding Frank-Wolfe Method

Lage Clara[1], Pustelnik Nelly[1], Arbona Jean-Michel[2], and Audit Benjamin[1]
[1] Univ Lyon, ENS de Lyon, CNRS, Laboratoire de Physique, F-69342 Lyon, France
[2] Univ Lyon, ENS de Lyon, CNRS, LBMC, F-69342 Lyon, France

February 15, 2024

Abstract

In this work, we focus on the challenging problem of designing an off-the-grid method for dictionaries involving both positional and scale shifts. To tackle this challenge, we introduce a novel algorithm inspired by the Sliding Frank-Wolfe approach. In our proposed algorithm, positions are treated as continuous variables, whereas scales are discretized. Such a strategy eliminates numerical instabilities inherent to the direct application of Sliding Frank-Wolfe. We successfully apply this algorithm to the study of DNA replication data.

1 Introduction

Formally, *sparse coding* methods consist in approximating a signal $z \in \mathcal{L}^2(\mathcal{X})$, in a vector space $\mathcal{X}$, by a finite linear combination of atoms selected from the dictionary $\mathcal{D} = \{\varphi(\cdot;\theta) \in \mathcal{L}^2(\mathcal{X}) \ : \ \theta \in \Theta\}$, where φ is a continuous mapping. The objective is to estimate the underlying unknown parameters $\bar{\theta}_1, ..., \bar{\theta}_K \in \Theta$, and amplitudes $\bar{\alpha}_1, ..., \bar{\alpha}_K \in \mathbb{R}$ modeling the signal z as:

$$z = \mathcal{F}\left(\sum_{k=1}^{K} \bar{\alpha}_k \varphi(\cdot;\bar{\theta}_k)\right),$$

where $\mathcal{F}$ denotes a stochastic degradation. This problem can be solved by different optimization techniques of sparse approximation [14, 18, 13].

Traditionally, *sparse coding* methods rely on the discretization of the parameter set Θ, corresponding to a set of $\widetilde{K}$ atoms $\{\varphi_k = \varphi(\cdot;\theta_k)\}_{k=1}^{\widetilde{K}}$, from which a small subset of $K > 0$ atoms must by chosen. In this context, LASSO (Least Absolute Shrinkage and Selection Operator, [18]) is a well accepted method that uses the ℓ_1 norm as a measure of sparsity. Numerically, the signal is a vector $\mathrm{z} \in \mathbb{R}^N$ as well as the atoms $\varphi_k \in \mathbb{R}^N$ and the LASSO is written as:

$$\widehat{a} \in \underset{a}{\mathrm{Argmin}} \ \|\mathrm{z} - \sum_{k=1}^{\widetilde{K}} a_k \varphi_k\|_2^2 + \lambda \|a\|_1, \tag{1}$$

where $\lambda > 0$, impacts the number of non-zero components of $a = (\hat{a}_k)_{1 \leqslant k \leqslant \widetilde{K}} \in \mathbb{R}^{\tilde{K}}$.

In this work, we focus on atoms φ for which the parametrization Θ is associated to dilatation and translation of a reference atom, forming a space $\times$ scale dictionary. We investigate how this type of dictionary interacts with sparse coding methods. As the translation of an atom can be expressed using a *convolution kernel* it gives rise to a variety of numerical methods. Particularly when Θ is discrete, these methods are called *convolutional sparse coding* and have been applied in audio processing and other fields [9, 22, 12, 17]. The popularity of these methods comes from (i) the possibility of providing a compact representation of a large dictionary, and (ii) the efficient computation of convolutions via FFTs.

Another objective of sparse coding methods is to increase the accuracy in the estimation of parameters. For this purpose, continuous sparse coding methods have shown significant advantages compared to traditional discretized formulations [3, 10]. This is the case of BLASSO (Beurling LASSO [19]), in which Θ equals $\mathcal{X}$. In BLASSO, the solution belongs to the space of measures $\mathcal{M}(\Theta)$ and is numerically approximated by a weighted sum of Dirac measures:

$$m = \sum_{k=1}^{K} \alpha_k \delta_{\theta_k}, \tag{2}$$

involving the weights $\alpha_k \in \mathbb{R}$ and $\theta_k \in \Theta$ elements of the parameter space where the measure is not zero. The optimization problem is given by:

$$\underset{m \in \mathcal{M}(\Theta)}{\text{minimize}} \ \|z - \Phi(m)\|_2^2 + \lambda |m|(\Theta), \tag{3}$$

where $|m|(\Theta)$ is the total variation of the measure m, [20, Section 6.1], $\lambda > 0$, and the operator Φ is defined as:

$$\begin{aligned} \Phi : \mathcal{M}(\Theta) &\longrightarrow \mathcal{L}^2(\Theta) \\ m &\longmapsto \int_{\Theta} \varphi(\cdot;\theta) \mathrm{dm}(\theta) = \sum_{k=1}^{K} \alpha_k \varphi(\cdot;\theta_k). \end{aligned}$$

The last equality holds when m is written as in (2). With some hypothesis on the regularity of the kernel φ, theoretical recovery guarantees have been established for BLASSO [19, 16, 6]. In the specific case of convolution kernels, numerically solving BLASSO can be performed efficiently using different methods [2, 7, 15]. For example, the Sliding Frank-Wolfe method [3, 15], based on the Frank-Wolfe method [11], transforms the non-constrained optimization problem (3) in a compact constrained problem where it is possible to apply the Frank-Wolfe algorithm. Sliding Frank-Wolfe method benefits from flexibility with respect to the space $\mathcal{X}$, and theoretical guarantees [15].

Contributions: We investigate BLASSO in the case of a space-scale transformation. In this context, we propose a new optimization method that combines continuous and discrete optimization allowing to reach spatial accuracy and good performance on scale recovery, without being sensitive to numerical instabilities. We also show that theoretical recovery guarantees of Sliding Frank-Wolfe algorithm are not affected in the hybrid model. The proposed algorithm is applied in the context of single molecule DNA replication studies [1]. Numerical tests show the adequacy and relevance of the hybrid method in estimating position (space) and speed (scale) with high precision.

Outline: In Section 2, we study the consequences of a space-scale dictionary in the original Sliding Frank-Wolfe algorithm. In Section 3, we present our hybrid algorithm, continuous in space and discrete in scale, highlighting the main theoretical differences between the proposed algorithm and original Sliding Frank-Wolfe. Finally, Section 4 presents a case study in the context of DNA replication with numerical experiments to support the relevance of the method.

2 Sliding Frank-Wolfe algorithm for space-scale parametrization

Space-scale setting – For a set $\mathcal{S} \subset \mathbb{R}$, we focus on a parameter space $\Theta = \mathcal{X} \times \mathcal{S}$. The dictionary set $\mathcal{D}$ is

$$\mathcal{D} = \left\{ \varphi(\cdot;(x,s)) = c_s \psi\left(\frac{\cdot - x}{s}\right), (x,s) \in \Theta \right\} \tag{4}$$

where the continuous function $\psi : \mathbb{R} \to \mathbb{R}$ is a reference atom and c_s, the normalizing constant, is such that $\|\varphi(\cdot,(x,s))\|_2 = 1$, for every $\theta = (x,s) \in \Theta$. When handling the discrete signal z, the variable $(\cdot)$ is replaced by a discretization space $\{u_i\}_{i=1}^N$ of the signal z. We consider the operator $\Phi\colon \mathcal{M}(\Theta) \to \mathcal{L}^2(\mathcal{X})$ such that

$$\Phi : m = \sum_{k=1}^{K} \alpha_k \delta_{(x_k,s_k)} \longmapsto \sum_{k=1}^{K} \alpha_k \varphi(\cdot;(x_k,s_k)).$$

In this context, the Sliding Frank-Wolfe algorithm (Section SIV), proposed on [15, Algorithm 2], provides a sequence with an accumulation point that minimizes problem (3). This accumulation point is approximated by $\{\alpha_k^*, s_k^*, x_k^*\}_{1\leqslant k\leqslant K}$ that defines the sum of Dirac measures $m^* = \sum_{k=1}^{N^*} \alpha_k^* \delta_{(x_k^*, s_k^*)}$.

For the iteration ℓ, let $\{\alpha^{[\ell]}, \theta^{[\ell]}\}$ define the set of amplitudes and spikes (space × scale), and $K^{[\ell]} = |\theta^{[\ell]}|$ be the number of spikes. The algorithm loops on three steps until it reaches the stopping criterion:
[Step 1] Estimate an additional spike $\bar{\theta}$ by maximizing

$$\eta^{\mathrm{SFW}}(\theta) = \left| \frac{1}{2\lambda} \langle \mathrm{z}(\cdot) - \Phi \left(\sum_{k=1}^{K^{[\ell]}} \alpha_k^{[\ell]} \delta_{\theta_k^{[\ell]}} \right), \varphi(\cdot, \theta) \rangle \right|, \tag{5}$$

and add $\bar{\theta}$ to the spike set, composed now by $K^{[\ell]} + 1$ spikes.
[Step 2] Adjust the amplitudes with the new set of spikes and obtain $\left\{\alpha^{[\ell+\frac{1}{2}]}, \theta^{[\ell+\frac{1}{2}]}\right\}$, where $\left|\theta^{[\ell+\frac{1}{2}]}\right| = K^{[\ell]} + 1$.
[Step 3] Solve the non-convex optimization problem (3) when restricted to a sum Dirac measures with $K^{[\ell]} + 1$ components. The initialization is made with the previous estimates. This step results on the refined parameters $\left\{\alpha^{[\ell+1]}, \theta^{[\ell+1]}\right\}$, where $K^{[\ell+1]} = \left|\theta^{[\ell+1]}\right|$.
Scale dictionary specificities – The optimization problem involved in **Step 1** relies on the gradient of η^{SFW} with respect to $\theta = (x, s)$, which may lead to numerical instabilities in the computation of $\nabla_x \eta^{\mathrm{SFW}}$. These instabilities are due to oscillations in the gradient $\nabla_x \psi(x = \tilde{x}, s)$, for a fixed $\tilde{x}$, when using a relatively large grid step $\nu = u_{i+1} - u_i$. A specific analysis is provided in the supplementary material. On the other hand, for $\tilde{s}$ fixed, $\nabla_x \eta^{\mathrm{SFW}}(x, s = \tilde{s})$ is well-behaved, motivating the hybrid scheme proposed in Section 3.

3 Hybrid continuous-discrete method

To solve the numerical instabilities that arise when the scale s is considered as a continuous parameter, we propose to reformulate problem (3) treating the scale parameter set as discrete. We consider $\widetilde{\Theta} = \mathcal{X} \times \widetilde{\mathcal{S}}$, where $\widetilde{\mathcal{S}} = \{s_1, ..., s_M\}$ denotes the discretization of $\mathcal{S}$ and for every $i \in \{1, \ldots, M\}$, we consider $m_i \in \mathcal{M}(\mathcal{X})$. The new formulation is given by:

$$\underset{m=(m_1,\ldots,m_M)}{\text{minimize}} \left\| \sum_{i=1}^{M} \Phi_i(m_i) - z \right\|_2^2 + \lambda \sum_{i=1}^{M} |m_i|(\mathcal{X}). \tag{6}$$

where $m_i = \sum_k \alpha_{i,k} \delta_{x_{i,k}}$, for $x_{i,k} \in \mathcal{X}$ and the operator $\Phi_i : \mathcal{M}(\mathcal{X}) \to \mathcal{L}^2(\mathcal{X})$ is defined as:

$$m_i = \sum_{k=1}^{K_i} \alpha_{i,k} \delta_{x_{i,k}} \mapsto \sum_{k=1}^{K_i} \alpha_{i,k} c_{s_i} \psi \left(\frac{\cdot - x_{i,k}}{s_i} \right). \tag{7}$$

This lead us to the hybrid discrete-continuous Algorithm 1.

The objective is to estimate the components $\{\alpha_{i,k}^*, x_{i,k}^*\}$, for $i \in \{1, ..., M\}$ of m_i^*, forming the solution $m^* = (m_1^*, ..., m_M^*)$. The index i incorporates the scale information. This algorithm loops on three steps: **[Step 1]** choose both the scale s_i and a first approximation of the translation component $x_{i,k}$ by maximizing η^{HSFW} **[Step 2]** adjust the amplitudes $\alpha_{i,k}$ based on the previously estimated $x_{i,k}$, for all i and k, and **[Step 3]** solve the non-convex optimization problem (3) with the operators Φ_i, $i \in \{1, ..., M\}$ defined by (7) to refine the parameters $\{\alpha_{i,k}, x_{i,k}\}$ starting from the previous estimates.

When atoms are not overlapping, steps (2)-(3) can focus only on the scale i chosen by Step 1. The algorithm employed on Steps 1 and 3 is L-BFGS-B. In Step 1, the problem is solved separately for each discrete scale variable. Step 2 is solved by FISTA [5, 4]. The stopping criterion of Algorithm 1 is specified line 3 of the algorithm.

The following theorem formalizes the fact that Algorithm 1 is the Frank-Wolfe algorithm applied to the hybrid formulation (6). With this result, Algorithm 1 benefits from the same convergence results than Frank-Wolfe method.

Theorem 1. *The Hybrid Sliding Frank-Wolfe (Algorithm 1) is the Frank-Wolfe Algorithm [11, 15] applied to problem* (6) *when* ϕ_i *are defined by* (7)*. In addition, if* $\psi \in KER^{(2)}$*, as defined in [15, Definition 4], any accumulation point (for the weak*-topology) of the sequence* $(m^{*,[\ell]})_{\ell\in\mathbb{N}}$ *obtained from the Algorithm 1 is in the set of minimizers of problem* (6)*.*

The proof is provided in Annex (Section 5).

4 Application to single molecule DNA replication data

Data description – One of the current goals in DNA replication studies is to characterize the location and the speed of the molecular motors responsible for DNA synthesis along the chromosomes. This can be achieved using DNA sequencing data [1] that captures the passage of the molecular motors by measuring the variation of the concentration of a chemical (BrdU, a modified nucleotide that incorporates in replacement of thymidines) as a function of the 1D coordinate along the chromosomes (Figure 1A). The molecular motors incorporate BrdU following its time-dependent intracellular level $\psi(t)$. $\psi(t)$ has been determined experimentally and follows an asymetrical wave pattern [1, Section Methods] defined in the supplementary material. The passage of the motors of constant speed s and passing position x at time 0 results in a 1D spatial pattern $\psi\left(\frac{\cdot - x}{s}\right)$ in the measured BrdU profile (Figure 1A). Hence, the faster the local replication speed, the longer the observed BrdU spatial wave (Figure 1B).

We note that ψ is not differentiable at the start of the wave and at the point of maximal BrdU concentration. This difficulty was overcome using directional derivatives that proved to be numerically well behaved when executing the Algorithm 1. In our discrete case, the normalization constant is approximated by $c_s = \frac{1}{\sqrt{s}\|\psi\|_2}$.

Experimentally, the BrdU concentration is determined with a spatial sampling period of 100 bp (base

---

Algorithm 1 Hybrid Sliding Frank-Wolfe (HSFW)

Initialization: Let $\lambda > 0$, $(\forall i)\ K_i^{[0]} \equiv 0$ and $x_i^{[0]} = \varnothing$.

1: **For** $\ell = 0, 1, \ldots$

2: **Step 1:** Estimate an additional spike:

$$(\bar{x}, \bar{i}) = \underset{\substack{x\in\mathcal{X}\\ i\in\{1,2,\ldots,M\}}}{\arg\max} \underbrace{\left| \frac{1}{2\lambda} \langle \mathrm{z} - \sum_{i=1}^{M} \sum_{k=1}^{K_i^{[\ell]}} \alpha_{i,k}^{[\ell]} c_{s_i} \psi\left(\frac{\cdot - x_{i,k}^{[\ell]}}{s_i}\right), \varphi_s(\cdot, x) \rangle \right|}_{\eta^{\mathrm{HSFW}}(x, s_i)}$$

and define $\begin{cases} x_{\bar{i}}^{[\ell+\frac{1}{2}]} = x_{\bar{i}}^{[\ell]} \cup \{\bar{x}\}, \\ x_i^{[\ell+\frac{1}{2}]} = x_i^{[\ell]} \text{ for all } i \neq \bar{i}, \\ K_{\bar{i}}^{[\ell+\frac{1}{2}]} = K_{\bar{i}}^{[\ell]} + 1, \\ K_i^{[\ell+\frac{1}{2}]} = K_i^{[\ell]} \text{ for all } i \neq \bar{i}. \end{cases}$

3: **If** $\eta^{\mathrm{HSFW}}(\bar{x}, s_{\bar{i}}) \leqslant 1$ **STOP**.

4: **Step 2:** Estimate the amplitudes using the elements of the spike-sets:

$$\alpha^{[\ell+\frac{1}{2}]} = \underset{\alpha}{\arg\min} \left\| \mathrm{z} - \sum_{i=1}^{M} \sum_{k=1}^{K_i^{[\ell+\frac{1}{2}]}} \alpha_{i,k} c_{s_i} \psi\left(\frac{\cdot - x_{i,k}^{[\ell+\frac{1}{2}]}}{s_i}\right) \right\|^2 + \gamma \|\alpha\|_1$$

5: **Step 3:** Determine a solution $m^{*,[\ell+1]}$ of the non-convex problem (6) restricted to Dirac measures m_i with $K_i^{[\ell+\frac{1}{2}]}$ spikes. The initialization is set to $\bar{m}_i = \sum_{k=1}^{K_i^{[\ell+\frac{1}{2}]}} \alpha_{i,k}^{[\ell+1/2]} \delta_{x_{i,k}^{[\ell+1/2]}}$ where $K_i^{[\ell+\frac{1}{2}]}$ denotes the number of spikes for scale s_i.

6: **Step 4:** Update for all $i : K_i^{[\ell+1]} = |m_i^{*,[\ell+1]}|$, $x^{[\ell+1]} = x^{*,[\ell+1]}$ and $\alpha^{[\ell+1]} = \alpha^{*,[\ell+1]}$

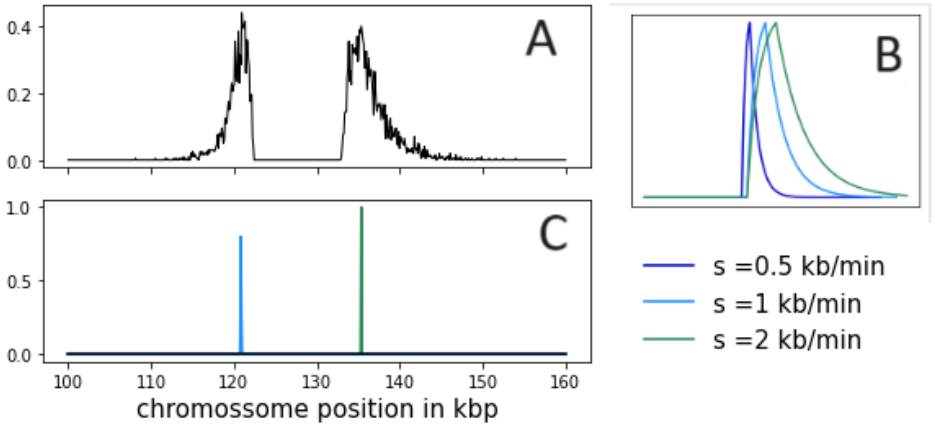

Figure 1: (A) Example of BrdU concentration signal along the chromossome with two divergent replication patterns. (B) 3 atoms of the dictionary. (C) Spikes of position and amplitude associated to the forks of signal (A).

pairs). This distance establishes the grid $\{u_i\}_{i=1}^N$ for the signal z (Section 2). In principle, the maximal spatial precision for x is 1 bp. Our goal is thus, considering the proposed off-the-grid method, to overcome the 100 bp sampling limit.

Experimental setting – We evaluate the performance of the proposed Hybrid Sliding Frank-Wolfe algorithm (Algorithm 1) with M-scales and compare them to a dictionary discretized both in time (position) and scale, thus with $\widetilde{K} = M \times N$ in (1). In our experiments we consider Matching Pursuit (MP) rather than LASSO as reference fully discrete method as it appears to be more efficient in this applicative context of very sparse representation. The experiments are run for $P = 200$ noisy signals and 200 noiseless signals $\mathrm{z}^{(p)} \in \mathbb{R}^N$. For each atom, position and speed are chosen according to a uniform distribution on [0,300] (kbp) and $[-3, -0.5] \cup [0.5, 3]$ (kbp/min) respectively. The stochastic degradation is assumed to follow a Poisson distribution with intensity parameter $\beta = 700$ to mimic the non-Gaussian experimental noise [1]. A fidelity term adapted to Poisson noise was tested in this context [8] and was not advantageous compared to the Euclidian norm, which explains our choice of distance. In experimental data, most signals have 1 or 2 atoms. Based on that, in our simulated data, signals have a maximum of 2 atoms.

For both approaches (hybrid and fully discrete), we compare the precision of position and velocity estimation by computing the mean absolute error compared to the ground truth. The choice of the parameter $\lambda = 0.001$ in Algorithm 1 is made in order to detect all the replication patterns.

Results – Figure 2 illustrates the performance of both hybrid (proposed HSFW) and discrete strategy (MP) when $M = 40$ for signal with one replication pattern. Both methods have a good behavior. A more accurate estimation of the position and amplitude of the atom is obtained with the HSFW as illustrated by the zoom. The MP solution is the constrained by grid step of 100 bp = 0.1 kb, while the hybrid solution is able to place the position between two grid elements.

In Figure 3, we compare the mean absolute error for discrete and hybrid methods with noisy and noiseless samples. As expected, increasing speed detection accuracy (increasing M) decreases position error. Note that the proposed HSFW systematically reduces the error from 20% up to 40% compared to MP for configurations with or without noise. We observe that for $M = 40$, MP achieves the optimal performance that can be obtained for a discrete method (black solid line) while the hybrid method overcomes this limit.

In Fig. 4 we display the scattered plot of the reconstruction error (i.e. $\|\mathrm{z} - \widehat{\mathrm{y}}_\bullet\|_2^2$) w.r.t the absolute position error for samples without noise and $M = 40$. The colors gradient represents the speed error. With HSFW (red), we observe that samples with low reconstruction error are those that have low position and speed error, allowing to easily select small absolute position/speed errors from the reconstruction error. With MP (blue), error in position are compensate by errors in speed resulting in a low reconstruction error but relatively high errors in the parameter estimations. The noisy samples exhibits a similar but less accurate behavior (results not shown).

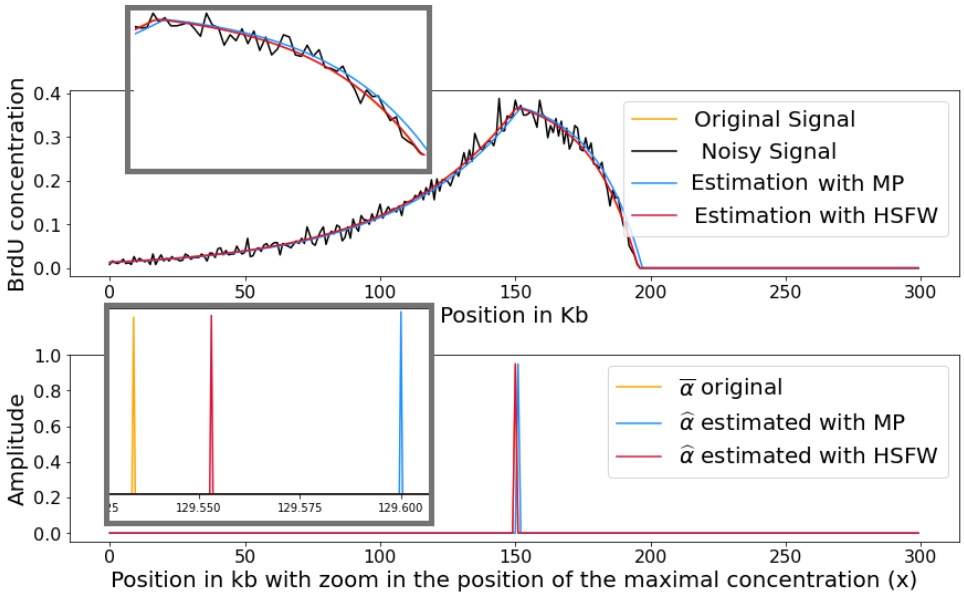

Figure 2: Example of a single replication fork fit, represented as in Figure 1 A,C. (First row) Reconstructed signals $\hat{y}_{\mathrm{MP}} = \sum_{k=1}^{\widetilde{K}} \hat{a}_k \hat{\varphi}_k$ (in blue) and $\hat{y}_{\mathrm{HSFW}} = \sum_{k=1}^{K} \hat{\alpha}_k \varphi(\cdot; \hat{\theta}_k)$ (in red). When zooming we can observe that the hybrid method is able to improve the resolution of position detection.

5 Annex : proof of Theorem 1.

The convergence proof is divided in four parts: (i) rewrite problem (6) with the aim of achieving a convex objective function with a different feasible set; (ii) prove the compactness of the feasible set; (iii) prove that the linear optimization (**Step 1** of Frank-Wolfe method [15]) can be written as **Step 1** of Algorithm 1; (iv) conclude that the sequence generated by Algorithm 1 has a convergent sub-sequence.

Following [15, Lemma 4], (6) can be reformulated as the convex optimization problem with an epigraphic constraint:

$$\min_{(m,t)\in\widetilde{\mathcal{C}}} \widetilde{T}_\lambda(m,t) := \left\| \sum_i \Phi_i(m_i) - z \right\|_2^2 + \lambda t \tag{8}$$

where

$$\widetilde{\mathcal{C}} = \left\{ (m_1, ..., m_M, t) \ : \ \sum_i |m_i|(\mathcal{X}) \leqslant t \leqslant \zeta \text{ and } \zeta = \frac{\|z\|^2}{\lambda} \right\}.$$

The upper bound ζ of $\widetilde{\mathcal{C}}$ is obtained applying $m_i = 0$ to (6).

One of the key points for applying *Frank-Wolfe* to problem (8) is to note that $\widetilde{\mathcal{C}}$ is a compact set in the weak*-topology. As mentioned for the Sliding Frank-Wolfe convergence [15, Remark 2], the ball in $\mathcal{M}(\mathcal{X})$ with the total variation metric is compact. We observe that $\widetilde{\mathcal{C}}$ is a closed set contained in the product of balls: $\Pi_{i\in\{1,..,M\}}\{m_i \ : \ |m_i|(\mathcal{X}) \leqslant \zeta\} \times \{t : 0 \leqslant t \leqslant \zeta\}$ which is compact by the Tychonoff's theorem, [21, Section 9.6, Theorem 1]), hence $\widetilde{\mathcal{C}}$ is compact.

The *Frank-Wolfe* algorithm consists in successive linear optimization problems in a convex and compact set. In our case, at iteration ℓ, the minimization is reformulated as follows:

$$\max_{(m,t)\in\widetilde{\mathcal{C}}} \sum_i \int_X \eta_i(x) \mathrm{d}m_i + \lambda t \tag{9}$$

where $\eta_i(x) = \frac{1}{2\lambda}\langle z - \Phi_i(m_i^{[\ell]}), \varphi_{s_i}(\cdot, x)\rangle$. Following [15, Remark 4], we shall compute the extremal points of the set $\tilde{\mathcal{C}}$ with the purpose of simplifying this minimization step. In our case, the extremal set of $\tilde{\mathcal{C}}$ can be

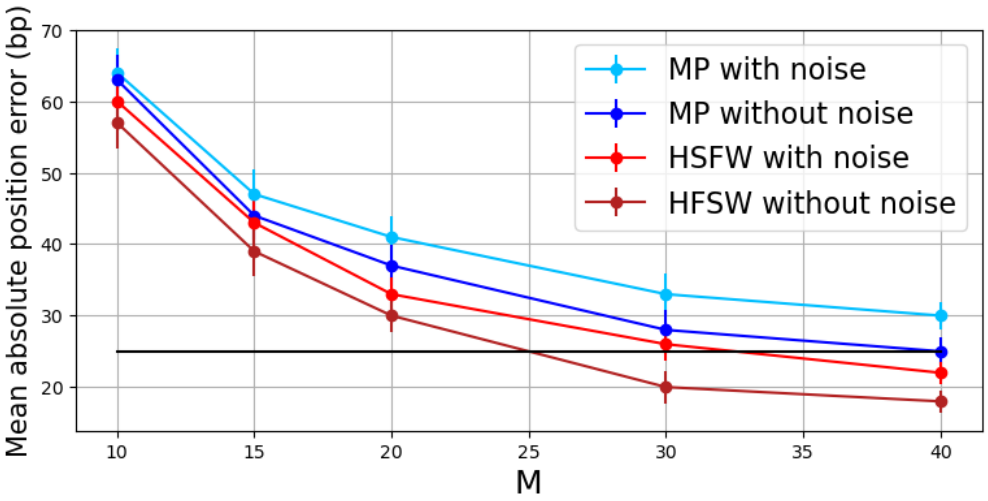

Figure 3: Mean absolute position error for MP/HSFW for noiseless/noisy regimes ($\beta = 700$). Black line: optimal mean position error for discrete methods with a grid step of 100 bp.

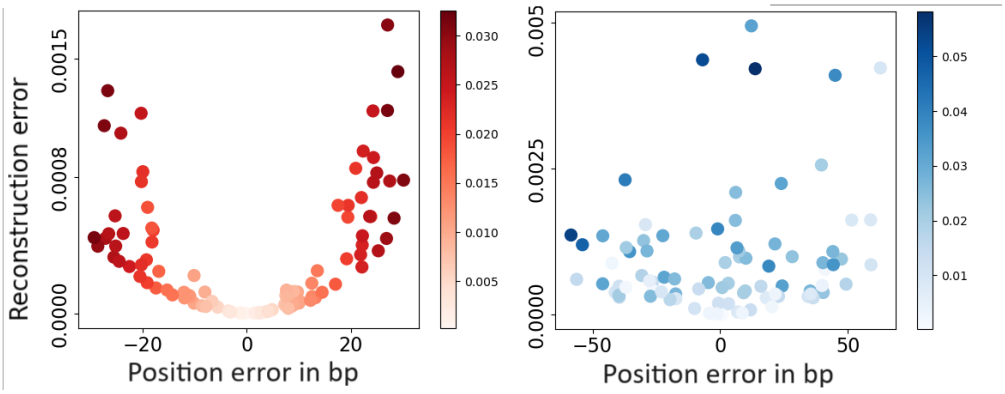

Figure 4: Scatter plot of the reconstruction error vs. position error for discrete (left) and continuous (right) methods when estimated without noise for $M = 40$. The color intensity of dots is given according to the absolute speed error.

easily computed as:

$$E(\tilde{\mathcal{C}}) = \{(m_1, ..., m_M, \zeta),\ m_i = 0,\ \text{for } i \neq i_0 \text{ and } m_{i_0} = \zeta\delta_x, \\ \text{for some } x \in \mathcal{X} \text{ and } i_0 \in \{1, ..., M\}\}.$$

Therefore, by (9), the sum of integrals becomes the value of $\eta_i(x)$, for some $x \in \mathcal{X}$, and for some $i \in \{1, ..., M\}$ leading to: $\underset{\{x \in X,\ i \in \{1,2,..,M\}\}}{\arg\max} |\eta_i(x)|$.

In addition, we observe that in Sliding Frank-Wolfe [15, Algorithm 2], the search step (see [15, Algorithm 1]) is replaced by any procedure able to decrease the value of the objective function. Therefore, we conclude that Algorithm 1 is the Frank-Wolfe algorithm applied to problem (6) and we can benefit from all convergence results of the later.

Following the steps of [15, Proposition 5], with the assumption that $\psi \in \text{KER}^{(2)}$, we conclude that the sequence $m^{*,[\ell]}$ is a bounded minimizing sequence. In addition, we observe that the objective function in (6) is l.s.c and convex to obtain that any accumulation point of $m^{[\ell]}$ is a solution to (6).

6 Conlusion

We propose a study of the Sliding Frank-Wolfe method for space $\times$ scale dictionaries. Numerical instabilities arise from the interaction of discretized signals with continuous optimization, specifically in the scale dependency of the dictionary. To address this limitation, we propose a hybrid algorithm dealing with space as a continuous variable and scale as a discrete variable. Compared to the MP algorithm, where the whole parameter space is discretized, our hybrid approach proves its efficiency and promising solution for DNA replication analysis.

This work was supported by the Agence Nationale de la Recherche (ANR-18-CE45-0002 and ANR-19-CE12-0028). We thank R. Gribonval for insightful discussions.

Supplementary material

7 Convolution kernel

In this work, we consider the *sparse coding* optimization problem for a parameter set $\Theta = \mathcal{X} \times \mathcal{S}$, where $\mathcal{X}$ represents a translation component:

$$\varphi(\cdot;\theta) = \varphi(\cdot;(x,s)) = \psi_s(\cdot - x). \tag{10}$$

When Θ is a discrete set, $\Theta = \{x_1, ..., x_N\} \times \{s_1, ..., s_M\}$, it is possible to write the problem in the convolutive form:

$$\widehat{b} \in \underset{b}{\text{Argmin}} \left\| \mathrm{z} - \sum_{i=1}^{M} b_i * \varphi_{s_i} \right\|_2^2 + \lambda \sum_{i=1}^{M} \|b_i\|_1,$$

where $\varphi_{s_i} \in \mathbb{R}^N$, and the sparse vectors $b_i \in \mathbb{R}^N$ encodes the discretized location and coefficients related to i-th atom.

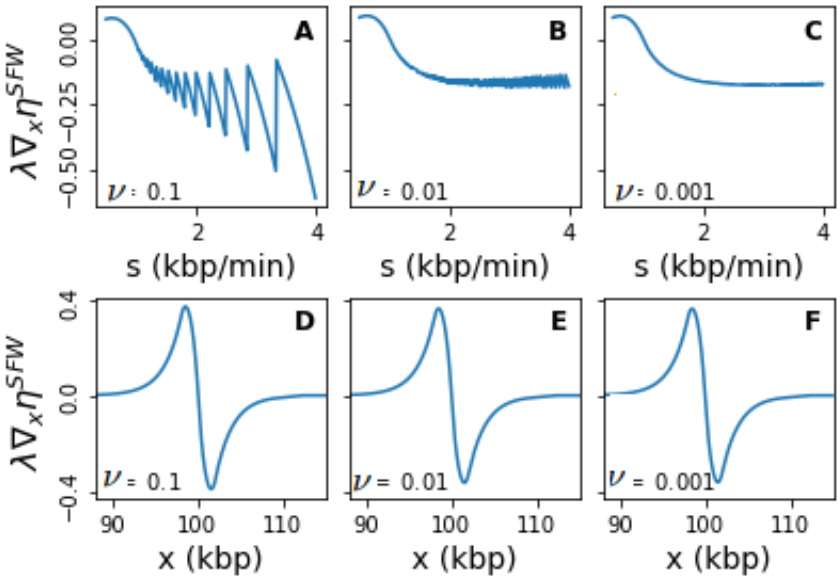

Figure 5: $\lambda \nabla_x \eta$ for DNA replication atoms for the first iteration of Sliding Frank-Wolfe Algorithm S1. We consider $\mathrm{z} = \varphi(\cdot, \overline{\theta})$, with $\overline{\theta} = (\overline{x}, \overline{s}) = (100 \text{ kbp}, 1 \text{ kbp/min})$, and grids $\{u_i\}_{i=1}^N$ with different step sizes $\nu = u_{i+1} - u_i$. (A,B,C) $\lambda \nabla_x \eta(x = \overline{x}, \cdot)$ as a function of s. (D,E,F) $\lambda \nabla_x \eta(\cdot, s = \overline{s})$ as a function of x.

8 Dictionary form:

The dictionary defined in (4) relies on a reference atom ψ. In the DNA replication application this function was determined experimentally [18] as:

$$\psi(t) = \begin{cases} c\left(1 - e^{-\frac{t+t_0}{\tau_1}}\right), & -t_0 \leqslant t \leqslant 0 \\ c\left(1 - e^{-\frac{t_0}{\tau_1}}\right) + \left(r - c\left(1 - e^{-\frac{t_0}{\tau_1}}\right)\right)\left(1 - e^{\frac{t}{\tau_2}}\right), & 0 \leqslant t \leqslant \infty \end{cases} \tag{11}$$

where the parameters τ_1, τ_2, a and c are assumed constant, with $\tau_1 = 0.8$ min, $\tau_2 = 1.4$ min, $c = 0.4$, $t_0 = 2$ min and $r = 0$. The parameter r represents the residual level of intracellular BrdU in the cell. The

value $r = 0$ is found in humans cells, while yeast presents higher values of r. The value of t_0 represents the duration of the BrdU pulse. Parameters τ_1 and τ_2 are related to the rate of import/export of BrdU by the cell. c controls the maximum level of BrdU. Since here $r = 0$ the function ψ decreases to zero for large values of t.

9 Gradient instability:

In Section II, we discuss the numerical instabilities on the first step of Sliding Frank-Wolfe (Algorithm 2), when considering scale dictionaries. This observation is illustrated when ψ has the form (11). In Figure 5, we observe the derivative $\nabla_x \eta(x = \widetilde{x}, s)$ and $\nabla_x \eta(x, s = \widetilde{s})$ for different values of the sampling period ν. They present oscillating behavior if s is not fixed. This problem is not specific to the function ψ in equation (11), and can also appear with other space-scale dictionaries described by (4).

10 Sliding Frank-Wolfe algorithm:

Algorithm 2 Sliding Frank-Wolfe

1: **Initialization:** Let $\lambda > 0$, $K^{[0]} = 0$, $\theta^{[0]} = \varnothing$

2: **For** $\ell = 0, 1, \ldots$

3: **Step 1:** Estimate an additional spike:

$$\bar{\theta} = \arg\max_{\theta \in \Theta} \eta^{\mathrm{SFW}}(\theta)$$

where:

$$\eta^{\mathrm{SFW}}(\theta) = \left| \frac{1}{2\lambda} \langle \mathrm{z} - \Phi \left(\sum_{k=1}^{K^{[\ell]}} \alpha_k^{[\ell]} \delta_{\theta_k^{[\ell]}} \right), \varphi(\cdot, \theta) \rangle \right|,$$

and define $\theta^{[\ell+\frac{1}{2}]} = \theta^{[\ell]} \cup \{\bar{\theta}\}$ and $K^{[\ell+\frac{1}{2}]} = K^{[\ell]} + 1$

4: **If** $\eta(\theta) \leqslant 1$ **STOP**.

5: **Step 2** Estimate the amplitudes by solving

$$\alpha^{[\ell+\frac{1}{2}]} = \arg\min_{\alpha} \left\| \mathrm{z} - \Phi \left(\sum_{k=1}^{K^{[\ell+\frac{1}{2}]}} \alpha_k \delta_{\theta_k^{[\ell+\frac{1}{2}]}} \right) \right\|_2^2 + \lambda \|\alpha\|_1$$

where $\theta \leftarrow \theta^{[l+\frac{1}{2}]}$.

6: **Step 3:** Estimate a solution m^* of (3) restricted to Dirac measures with $K^{[\ell+\frac{1}{2}]}$ spikes. The initialization is set to $\overline{m} = \sum_{k=1}^{K^{[\ell+\frac{1}{2}]}} \alpha_k^{[\ell+\frac{1}{2}]} \delta_{\theta_k^{[\ell+\frac{1}{2}]}}$.

Update: $K^{[\ell+1]} = |\theta^{[l+1]}|$, $\theta^{[l+1]} = \theta^*$ and $\alpha = \alpha^*$.

References

[1] B. Theulot et al. "Genome-wide mapping of individual replication fork velocities using nanopore sequencing". In: *Nature Communications* 13 (2022). DOI: 10.1038/s41467-022-31012-0.

[2] J.-M. Azaïs, Y. de Castro, and F. Gamboa. "Spike detection from inaccurate samplings". In: *Applied and Computational Harmonic Analysis* 38.2 (2015), pp. 177–195.

[3] L. Blanc-Féraud B. Laville and G. Aubert. "Off-The-Grid Variational Sparse Spike Recovery: Methods and Algorithms". In: *Journal of Imaging* 7.12 (2021). ISSN: 2313-433X. DOI: 10.3390/jimaging7120266. URL: https://www.mdpi.com/2313-433X/7/12/266.

[4] A. Beck and M. Teboulle. "A fast Iterative Shrinkage-Thresholding Algorithm with application to wavelet-based image deblurring". In: *2009 IEEE International Conference on Acoustics, Speech and Signal Processing*. 2009, pp. 693–696. DOI: 10.1109/ICASSP.2009.4959678.

[5] P. Lu C. Zhu R. Byrd and J. Nocedal. "Algorithm 778: L-BFGS-B: Fortran Subroutines for Large-Scale Bound-Constrained Optimization". In: *ACM Trans. Math. Softw.* 23.4 (1997), 550–560. ISSN: 0098-3500. DOI: 10.1145/279232.279236. URL: https://doi.org/10.1145/279232.279236.

[6] E. Candès and C. Fernandez-Granda. "Super-Resolution from Noisy Data". In: *Journal of Fourier Analysis and Applications* 19 (2013), pp. 1229–1254. DOI: 10.1007/s00041-013-9292-3.

[7] L. Chizat. "Sparse Optimization on Measures with Over-parameterized Gradient Descent". In: *Mathematical Programming* 194 (2021). DOI: 10.48550/ARXIV.1907.10300.

[8] *Codage espace-échelle parcimonieux en présence de bruit non-gaussien. Application à l'analyse de la réplication de l'ADN en molécule unique.)* 2023.

[9] L. Dragoni. "Spike sorting for massive neurophysiological datasets : sliding window working set strategy for the estimation of convolutional models in high dimension". PhD thesis. 2022.

[10] C. Soussen E. Clément R. Gribonval and C. Herzet. "OMP and Continuous Dictionaries: Is k-step Recovery Possible?" In: *IEEE International Conference on Acoustics, Speech and Signal Processing (ICASSP)*. 2019, pp. 5546–5550. DOI: 10.1109/ICASSP.2019.8683617.

[11] E. Levitin and B. Polyak. "Constrained minimization methods". In: *USSR Computational Mathematics and Mathematical Physics* 6.5 (1966), pp. 1–50. ISSN: 0041-5553. DOI: https://doi.org/10.1016/0041-5553(66)90114-5.

[12] M. Schmidt M. Mørup and L. Hansen. *Shift Invariant Sparse Coding of Image and Music Data*. Tech. rep. 2008.

[13] S. Mallat and Z. Zhang. "Matching pursuits with time-frequency dictionaries". In: *IEEE Trans. Signal Process.* 41 (1993), pp. 3397–3415.

[14] B. Natarajan. "Sparse Approximate Solutions to Linear Systems". In: *SIAM Journal on Computing* 24.2 (1995), pp. 227–234. DOI: 10.1137/S0097539792240406.

[15] G. Peyré Q. Denoyelle V. Duval and E. Soubies. "The sliding Frank–Wolfe algorithm and its application to super-resolution microscopy". In: *Inverse Problems* 36.1 (2019), p. 014001. DOI: 10.1088/1361-6420/ab2a29.

[16] V. Duval Q. Denoyelle and G. Peyré. "Support Recovery for Sparse Deconvolution of Positive Measures". In: *Journal of Fourier Analysis and Applications* 23.5 (2016), pp. 1153–1194.

[17] H. Kwong R. Grosse R. Raina and Y. Andrew. "Shift-Invariant Sparse Coding for Audio Classification". In: *Proceedings of the Twenty-Third Conference on Uncertainty in Artificial Intelligence*. Arlington, Virginia, USA: AUAI Press, 2007, 149–158. ISBN: 0974903930.

[18] R. Tibshirani. "Regression Shrinkage and Selection via the Lasso". In: *Journal of the Royal Statistical Society. Series B (Methodological)* 58.1 (1996), pp. 267–288. ISSN: 00359246.

[19] D. Vincent and G. Peyré. "Exact Support Recovery for Sparse Spikes Deconvolution". In: *Foundations of Computational Mathematics* 15.5 (2015), pp. 1315–1355. DOI: 10.1007/s10208-014-9228-6.

[20] R. Walter. *Real and Complex Analysis, 3rd Ed.* USA: McGraw-Hill, Inc., 1987. ISBN: 0070542341.

[21] A. Wilansky. *Functional Analysis*. Blaisdell Publishing, 1964.

[22] Y. Zhu and S. Lucey. "Convolutional Sparse Coding for Trajectory Reconstruction". In: *IEEE Transactions on Pattern Analysis and Machine Intelligence* 37.3 (2015), pp. 529–540. DOI: 10.1109/TPAMI.2013.2295311.